Electrochemical Generation of Catalytically Active Edge Sites in C₂N-Type Carbon Materials for Artificial Nitrogen Fixation

*Wuyong Zhang, Shaoqi Zhan, Qing Qin, Tobias Heil, Xiyu Liu, Jinyeon Hwang, Thimo H. Ferber, Jan P. Hofmann, and Martin Oschatz**

The electrochemical nitrogen reduction reaction (NRR) to ammonia (NH_3) is a potentially carbon-neutral and decentralized supplement to the established Haber–Bosch process. Catalytic activation of the highly stable dinitrogen molecules remains a great challenge. Especially metal-free nitrogen-doped carbon catalysts do not often reach the desired selectivity and ammonia production rates due to their low concentration of NRR active sites and possible instability of heteroatoms under electrochemical potential, which can even contribute to false positive results. In this context, the electrochemical activation of nitrogen-doped carbon electrocatalysts is an attractive, but not yet established method to create NRR catalytic sites. Herein, a metal-free C_2N material (HAT-700) is electrochemically etched prior to application in NRR to form active edge-sites originating from the removal of terminal nitrile groups. Resulting activated metal-free HAT-700-A shows remarkable catalytic activity in electrochemical nitrogen fixation with a maximum Faradaic efficiency of 11.4% and NH_3 yield of 5.86 µg mg$^{-1}_{cat}$ h^{-1}. Experimental results and theoretical calculations are combined, and it is proposed that carbon radicals formed during activation together with adjacent pyridinic nitrogen atoms play a crucial role in nitrogen adsorption and activation. The results demonstrate the possibility to create catalytically active sites on purpose by etching labile functional groups prior to NRR.

1. Introduction

NH_3 is one of the most important chemicals in the world. It has an annual global production volume of approximately 175 million tons[1] and is a pivotal feedstock for producing fertilizers and medicals. Its consumption is ever-increasing with the rapid development of modern society.[2] Until now, the industrial production of ammonia is still highly dependent on the prestigious Haber-Bosch process, which operates under harsh conditions (300–500 °C and 150–300 atm) and requires the use of purified hydrogen-containing synthesis gas, accounting for more than 1% of the global energy consumption. With every ton of NH_3 produced, more than one ton of CO_2 is generated.[3] Furthermore, Haber-Bosch is a highly centralized process and transportation of ammonia and fertilizers to the final consumers creates additional challenges, energy consumption, and pollution.[4] Therefore, it is highly desirable to develop

W. Zhang, Q. Qin, T. Heil, J. Hwang, M. Oschatz
Max Planck Institute of Colloids and Interfaces
Department of Colloid Chemistry
Am Mühlenberg 1, 14476 Potsdam, Germany
E-mail: martin.oschatz@uni-jena.de

W. Zhang, M. Oschatz
Center for Energy and Environmental Chemistry Jena (CEEC Jena)
Institute for Technical Chemistry and Environmental Chemistry
Friedrich-Schiller-University Jena
Philosophenweg 7a, 07743 Jena, Germany

S. Zhan
Department of Chemistry
University of California
Riverside, CA 92521, USA

X. Liu
Hefei National Laboratory for Physical Sciences at the Microscale
Collaborative Innovation Center of Chemistry for Energy Materials
School of Chemistry and Materials Science
University of Science and Technology of China
Hefei, Anhui 230026, P. R. China

T. H. Ferber, J. P. Hofmann
Surface Science Laboratory
Department of Materials and Earth Sciences
Technical University of Darmstadt
Otto-Berndt-Strasse 3, 64287 Darmstadt, Germany

alternative decentralized processes for ammonia synthesis that could run in simple reactors and under less harsh conditions. In ideal case such a process would be driven by energy from renewable sources.[5] The combination of NH_3 synthesis with renewable electricity is a necessary requirement for a future CO_2-free chemical industry.

Electrochemical reduction of nitrogen (N_2) therefore seems to be an alternative worthy exploring.[6] However, electrocatalytic activation of the chemically highly inert dinitrogen molecule is a difficult task. Moreover, the strong competition between hydrogen evolution reaction (HER) and NRR further lowers the efficiency due to selectivity limitations caused by the nearly similar redox potential (0 V and 0.094 V versus RHE for HER and NRR, respectively).[7] NRR to NH_3 is a 6-electron transfer process with many kinetic barriers and configurational requirements resulting in high activation overpotential. Alternative reactor and electrolyte concepts have been proposed to overcome these limitations,[8] but it is a matter of fact that the development of novel catalytic nanomaterials with high energy adsorption sites for nitrogen activation is currently the top priority on the road towards an NRR system with practically relevant space-time-yield and energy efficiency.[9] Numerous nanomaterials including metals, metal oxides, metal chalcogenides and metal-free carbon materials have been developed and successfully applied as electrocatalysts for NRR over the past years.[10] However, these developments seem to have reached their technical and conceptual boundaries and no giant leap can be anticipated for future research.[11] At this tipping point of potential stagnation, novel and unconventional catalytic concepts and electrode/reactor designs for the electrochemical activation of nitrogen are needed, which consider the microkinetic and macrokinetic demands at the same time.[12] Notably, NRR results or comparable catalytic materials can show significant differences between laboratories.[10h,13] It can be anticipated that one of the most straightforward ways to overcome such experimental limitations in the future will be to move to reactor concepts with larger solid-liquid-gas interfaces and therefore intrinsically higher ammonia production rate.[14]

Among the catalytic nanomaterials investigated, metal-free carbon-based materials have attracted a lot of attention because of their abundancy and low-cost.[15] Especially heteroatom-rich carbons (e.g., carbons doped with nitrogen) emerged as promising NRR catalysts recently and different mechanisms for the activation of N_2 on their surface have been proposed.[10a,16] Nonetheless, carbon materials seem to be constantly on the trailing end of the activity race compared with metal-based materials. The first reason for this might be their possibly lower intrinsic density of catalytically active sites. While in a nanostructured metal-based catalyst in principle every surface atom could act as an active center, part of the atoms in carbon-based materials are needed to "create" catalytically active sites and are therefore not active themselves. Secondly, the actual role of heteroatoms and the chemical construction of catalytically active sites are still not understood in detail. Porous nitrogen-doped carbon materials are often comparably heterogeneous in structure and precise tailoring of their chemical architecture is a difficult task. The controlled synthesis of such metal-free catalysts therefore remains a major challenge.[17] While heteroatom doping seems to be an effective route to improve

electrochemical activity of carbon materials by regulating the local distribution of electron density,[10,16a,18] it is often observed that the stability of heteroatoms under electrocatalytic reaction conditions is another severe limitation. Especially if nitrogen-doped carbons are applied in NRR, false positive results can be obtained and misinterpretations can be made when unstable nitrogen species are released from catalysts themselves and detected as ammonia in the reaction solution.[7b,19] However, the amount of detected ammonia in such cases often still exceeds the amount of nitrogen in the catalysts. When other analytical issues or contaminations can be ruled out, such findings indicate that the removal of electrochemically unstable nitrogen-containing functional groups from nitrogen-doped carbons could be responsible for the formation of catalytically active areas serving as strong adsorption sites for dinitrogen suitable for NRR. Related catalyst engineering strategies have already been recently applied to polymeric carbon nitrides. Controlled thermal generation of nitrogen vacancies was found to be a suitable method for the activation of N_2 due to bonding with electron back-donation.[10a,18a] In these cases, nitrogen atoms from the backbone of the carbon nitrides did not contribute to ammonia production. Comparable "defect engineering" is not limited to carbon-based materials. For instance, it was also successfully applied to hybrid metal-oxide based materials, such as oxygen-vacancy-rich $TiO_2/Ti_3C_2T_x$ (with T = OH or -F)[20] or defect-rich amorphous $Bi_4V_2O_{11}/CeO_2$.[21] In both cases, the availability of localized electrons and thus the ability for π-back donation is enhanced, which can contribute to dinitrogen activation. In all these examples, however, the potential catalytically active sites are supposedly created with the synthesis of catalysts, that is, before the materials are engineered into an electrode and transferred to the reaction medium. A look at the field of classical thermal catalysis shows that the activation of catalysts to create the desired active phase within the actual reactor under conditions close to the later catalytic process is widely established there.[22] Although such in situ activation comes with a couple of advantages like the avoidance of contact between the catalysts and air or solvents and although electrochemical activation most likely occurs accidentally in many cases, a comparable concept is yet neither widely understood nor systematically established in electrocatalysis. A few examples for electrocatalytic activation of metal-based catalysts have been reported but a comparable approach has not yet been established for metal-free materials in NRR.[23]

Herein, a C_2N-type nitrogen-rich carbon material with high concentration of pyrazinic nitrogen and terminal nitrile groups was employed as model material to investigate the possibility for electrochemical activation of an NRR catalyst. C_2N-type materials have been reported before but their application for novel electrocatalytic mechanisms remained so far unexplored to the best of our knowledge.[24] Accompanied by the electrochemical etching of unstable nitrile groups, C_2N went through an unexampled activation process to form activated C_2N. After activation, the materials exhibit excellent NRR performance with the highest Faradaic Efficiency (FE) of 11.4% and an NH_3 yield of 5.86 μg mg^{-1}_{cat} h^{-1}. Unlike traditional synthetic processes, such a unique electrochemical process modifies and rebuilds the material surface, decorating the porous structure with well-defined and homogenous active edge sites.

**ADVANCED
SCIENCE NEWS**

www.advancedsciencenews.com

NANO · MICRO

small

www.small-journal.com

Furthermore, supported by DFT calculations, a corresponding NRR mechanism based on a synergistic effect between carbon radicals and adjacent pyrazinic nitrogen atoms is proposed.
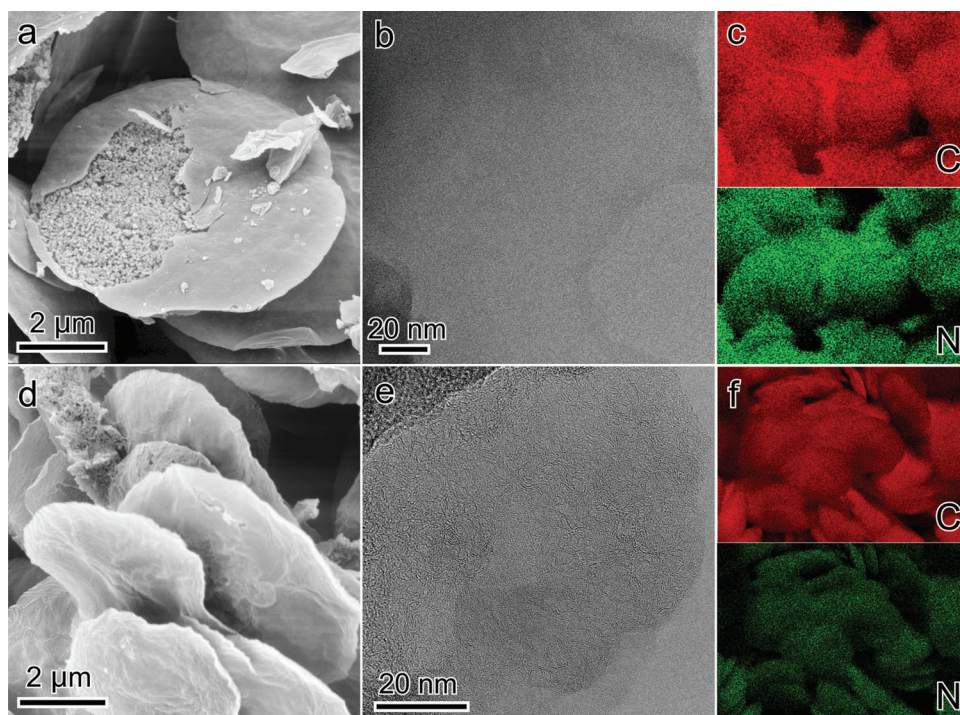
2. Results and Discussion

Porous C_2N was synthesized by direct thermal condensation of hexaazatriphenylene-hexacarbonitrile (HAT-CN) under N_2 atmosphere at different temperatures according to a previous report.[25] Resulting materials are denoted as HAT-700 and HAT-950 corresponding to their synthesis temperature. The microstructure of as-obtained HAT-Ts was studied by scanning electron microscopy (SEM) and both samples show a plate-like structure with a diameter of ~5 µm. The internal parts of the partly opened disks of HAT-700 consist of small, aggregated particles (**Figure 1**a,d). In contrast, HAT-950 has a closed shell without obvious defects. The porous structures of HAT-Ts can also be observed in high-resolution transmission electron microscopy (HRTEM, Figure 1b,e). HAT-950 has more graphitic structure in comparison to HAT-700. This is characteristic for the typical ongoing carbon ordering at higher condensation temperature.[25]

X-ray diffraction (XRD) patterns display a broad peak centered at around 26° (2 Theta) which is attributed to carbon (002) diffraction (Figure S1, Supporting Information).[26] Energy-dispersive X-ray (EDX) mapping confirms the homogenous distribution of carbon and nitrogen atoms in HAT-Ts. HAT-700 apparently has a higher heteroatom content as indicated by the intense response in nitrogen mapping (Figure 1c,f). The quantitative element content was analyzed by combustion elemental analysis (EA), EDX and X-ray photoelectron spectroscopy (XPS). All applied methods (Table S1, Supporting Information) show that HAT-700 has a higher content of nitrogen and a lower C/N atomic ratio in comparison to HAT-950. The porosity of HAT-Ts was investigated by nitrogen physisorption experiments (Figure S2a, Supporting Information). HAT-700 has a specific surface area (631 m^2 g^{-1}), which is comparable to HAT-950 (564 m^2 g^{-1}). Besides, the different adsorption behaviors of both samples indicate variations in their pore architectures. HAT-700 has a type I(a) isotherm as typical for materials with narrow micropores. In contrast, HAT-950 exhibits a type IV(a) isotherm with the hysteresis loop of H4 type and large uptake of nitrogen at high relative pressure, as expected for materials with large mesopores.[27] Accordingly, the pore size distributions of HAT-Ts analyzed by the quenched-solid density functional theory (Figure S2b, Supporting Information) indicate that HAT-700 mainly consist of micropores with diameters below 2 nm whereas HAT-950 has more mesopores spanning from 2 to 10 nm in diameter.

HAT-Ts have been chosen as model substances for the following investigations because not only their pore structure but also their atomic construction (here in particular the content and chemical bonding motives of the nitrogen atoms as well as the concentration of uncondensed nitrile functional groups) can be controlled by the condensation temperature. The binding energies of nitrogen, carbon, and oxygen 1s electrons within HAT-Ts were further investigated by XPS (Figure S3a, Supporting Information). From the deconvoluted high-resolution C 1s spectra (Figure S3b, Supporting Information), it can be seen that the relative content of electron-rich graphite-like sp^2 carbon with BE(C 1s) centered at 284.8 eV significantly increases from 9.2 at% for HAT-700 to 37.8 at% for HAT-950, accompanied by the decrease of the relative content of sp^2-carbon bonded to


Figure 1. a,d) SEM, b,e) HRTEM, and c,f) EDX mapping images for a–c) HAT-700 and d–f) HAT-950.

ADVANCED
SCIENCE NEWS
www.advancedsciencenews.com

NANO · MICRO
small
www.small-journal.com

more electronegative nitrogen (BE(C 1s) centered at 286.2 eV) from 68.2 at% to 47.1 at%. The N1s spectrum of HAT-950 is less intense compared to HAT-700 due to the decrease of nitrogen content (Figure S3c, Supporting Information). Further deconvolution shows that the peak at lower binding energies of BE(N 1s) in the range of 398–399 eV attributed to nitrile- and pyrazine groups decrease in intensity, whereas quaternary nitrogen atoms with BE(N 1s) = 400–401 eV become more dominant in HAT-950.[28] In contrast to carbon and nitrogen, there is not such an obvious difference in O 1s speciation between HAT-700 and HAT-950 (Figure S3d, Supporting Information).

Nitrogen-doped carbon materials have been successfully applied in NRR and other electrocatalytic reactions,[10a,18a,29] but it is a matter of fact that their intrinsic heterogeneity makes it difficult to achieve a detailed understanding for the source of catalytic activity and especially for the possible contribution of an electrochemical activation. HAT-Ts are generally also expected to be active as NRR electrocatalysts. In the fundamental scientific context, they can serve as ideal model compounds, because their nitrogen content, binding motives of the heteroatoms, and the chemistry of the edge sites can be controlled by the condensation temperature. For that purpose, as-synthesized HAT-Ts loaded on carbon paper (1 mg cm^{-2}) were employed as working electrode for nitrogen reduction in 0.1 M HCl electrolyte with a three-electrode system (Figure S4, Supporting Information). Cyclic voltammetry (CV) was measured first on electrodes with a wide potential range until the response curve became stable. An unexpected progressive current increase, which appeared for HAT-700 during continued cycling, indicates a change of its chemical structure over time (Figure S5, Supporting Information). In contrast, a decrease of current density was observed for HAT-950 which has a lower total nitrogen-content and contains heteroatoms that are electrochemically more stable. To further investigate the electrochemical behavior of both materials under CV etching, tests with 2000 cycles at a rate of 100 mV s^{-1} were carried out with HAT-700 in an argon-saturated electrolyte. As expected, the electrochemical response of HAT-700 increased dramatically under cycling (Figure S6, Supporting Information). After CV etching, the obtained activated HAT-700 (denoted as HAT-700-A) exhibited not only an increased response current, but also a shift of its onset potential by 570 mV in linear sweep voltammetry (LSV, Figure S7, Supporting Information) in presence of nitrogen. These measurements point towards an improved conductivity and/or the generation of electrocatalytically active sites, which is also proven by the weakened interfacial charge-transfer resistance in the electrochemical impedance spectroscopy (EIS, Figure S8, Supporting Information). In comparison, there is only a negligible change of the LSV curve of HAT-950 (Figure S7b, Supporting Information) even after the CV treatment. These results indicate a significant irreversible change of the structure of HAT-700 during this electrochemical procedure. Given the fact that both samples differ in their content of nitrile groups, the most likely reason is the electrochemical etching of these abundant edge-functionalities in HAT-700. In the next step, the NRR activity of HAT-700-A in aqueous electrolyte has been tested. HAT-700-A exhibits intense response to nitrogen with higher current density from −0.50 V to −1.10 V versus RHE in N$_2$-saturated electrolyte than in Ar-saturated electrolyte (**Figure 2**a). Several control experiments were subsequently performed to quantify the NRR products and clarify their origin (Figure 2b). Under the given conditions, limited or no ammonia was detected by the indophenol blue method under Ar atmosphere, at open circuit voltage and unaided carbon paper electrode.[30] On the contrary, strong absorption of indophenol blue was observed when HAT-700-A was set under electrochemical potential in the presence of nitrogen. This indicates that ammonia is generated from the electroreduction of dissolved N$_2$. Furthermore, the yields of ammonia and the corresponding Faradaic efficiencies (FEs) at all given potentials are plotted according to a NH$_4^+$ standard curve (Figure S9, Supporting Information). HAT-700-A exhibits a maximum FE of 11.4% toward ammonia at −0.60 V versus RHE and the maximum ammonia production rate reaches 5.86 µg mg$^{-1}_{cat}$ h^{-1} at −0.70 V versus RHE (Figure 2c). The response current increases with more negative applied potential, but, in agreement with other studies, this leads to the pronounced dominance of HER (Figure S10, Supporting Information). NRR performance was further validated by nuclear magnetic resonance (NMR) spectroscopy (Figure S11, Supporting Information). At the point of −0.60 V versus RHE, NRR performance determined by NMR showed consistency with the FE and NH$_3$ production rate determined by the indophenol blue technique (Figure S12, Supporting Information). No hydrazine was detected during the NRR process at all given potentials (Figure S13, Supporting Information), demonstrating a typical high nitrogen selectivity of HAT-700-A. The NRR activity of HAT-950 was also tested and compared with HAT-700-A (Figure S14, Supporting Information). A maximum FE of 4.2% at −0.40 V versus RHE can be achieved with a maximum ammonia production rate of 3.2 µg mg$^{-1}_{cat}$ h^{-1} which are both inferior to HAT-700-A. Notably, HAT-950 has a slightly lower overpotential, which can be attributed to its better electronic conductivity. An electrochemical stability test of HAT-700-A (Figure S15, Supporting Information) shows that the material can produce ammonia over 24 h and that the microstructure of the materials particles does not significantly change after this procedure (Figure S16, Supporting Information). A slight deviation of the NH$_3$ production over time can be observed after more than 8 h of reaction, which may be attributed to crossover of a part of the produced ammonium from cathode to anode or to a decrease of the FE over time resulting from blocking of the NRR active sites with ammonium (Figure S17, Supporting Information). The materials have further been tested for five-consecutive NRR cycles and there is only a slight fluctuation of FE and NH$_3$ production rate observed during the cycles (Figure S18, Supporting Information), further revealing the stability of HAT-700-A.

As it has been reported recently, numerous factors could influence the reliability of NRR results such as impurities in the supplied N$_2$ (NH$_3$, NO$_x$, or others) or residual nitrogen-containing compounds in the water and glass container.[19a,b,d] To minimize their effect on NRR results, gas-scrubbing bottles were used in all experiments to remove possible impurities from the supplied nitrogen. The results reported here have been obtained with N$_2$ gas from a central house supply, the purity of which may slightly vary over time. We have therefore repeated the experiments with nitrogen gas of 99.999% purity and measured possible other nitrogen sources in the reaction
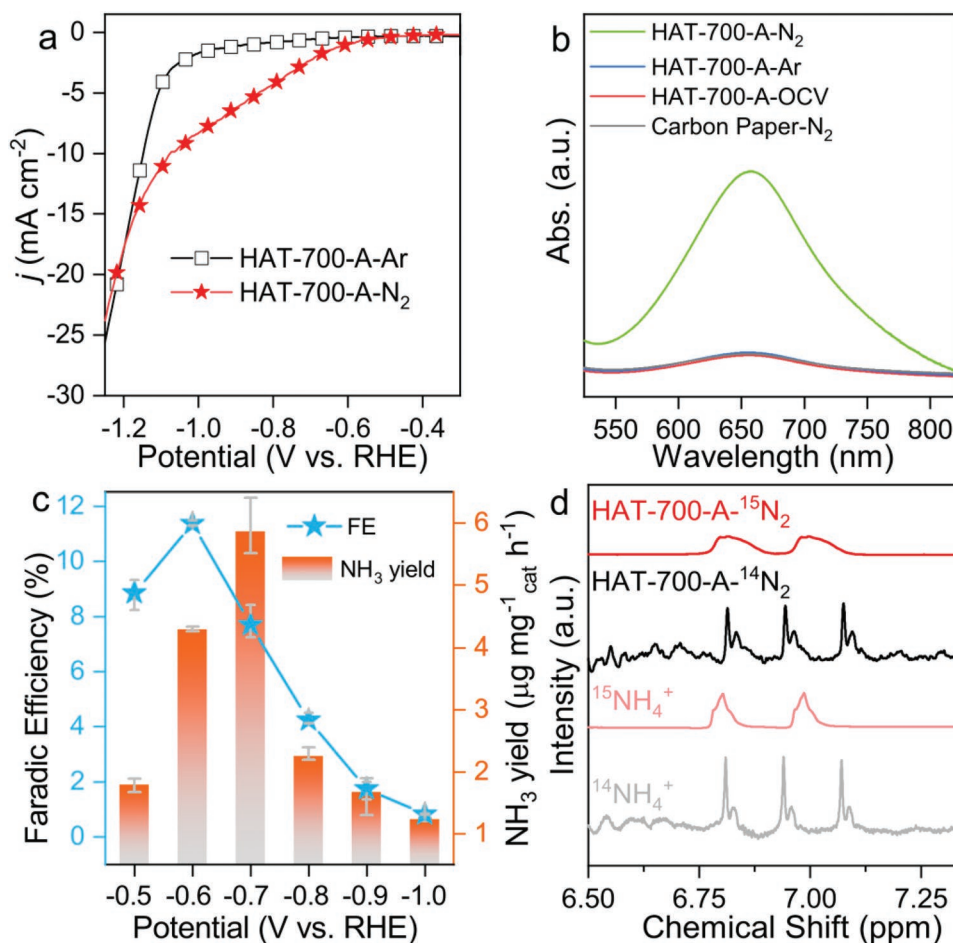
Figure 2. a) LSV of HAT-700-A under Ar and N_2 flow. b) Control experiments evaluated by the indophenol blue method. c) FE and NH_3 yield of HAT-700-A at all given potentials. d) ^1H NMR spectra of standard samples of $^{14}NH_4Cl$ and $^{15}NH_4Cl$ (light line) and pre-concentrated electrolytes from NRR with $^{14}N_2$ and $^{15}N_2$ as supplied gases (dark line).

solution. For the latter, nitrate and nitrite UV–Vis analysis have been performed for the fresh electrolyte, after supplying N_2 gas with and without scrubbing as well as after leaving the cell open overnight (Figure S19, Supporting Information). For both anions, no increase of the concentration in comparison to the as-made electrolyte has been detected with or without the application of gas scrubbing. In accordance with the recommended rigorous testing protocols for NRR we believe that proper gas scrubbing is of huge importance to get reliable results and to minimize the risk to get false positive results in electrochemical nitrogen reduction. For the present study, however, we were not able to detect extreme differences in our electrochemical results with or without nitrogen scrubbing. The electrochemical experiments have been further repeated with nitrogen gas of a nominal purity of 99.999% and the result is comparable to those obtained by the application of N_2 from the central supply (Figure S20, Supporting Information). Besides, isotope labeling experiments with $^{15}N_2$ as the feeding gas that also went through a scrubbing procedure have been performed to further validate the nitrogen source for ammonia. From the ^1H NMR spectra of pre-concentrated electrolyte after electrolysis with different N_2 gases employed (Figure 2d), distinct doublet peaks of $^{15}NH_4^+$ with a spacing of 73 Hz were observed, while triple peaks of

$^{14}NH_4^+$ with 52 Hz spacing can be detected after the supply of $^{14}N_2$. In combination with the continuous production of ammonia under N_2 flow with electric potential, it is confirmed that the measured NH_3 originates from the electroreduction of N_2 dissolved in the electrolyte. Quantitative analysis of the isotope labelling experiment also shows that the FE result with $^{15}N_2$ is comparable to that of $^{14}N_2$ at −0.6 V versus RHE (Figure S21, Supporting Information).

Motivated by the novel electrochemical activation process of HAT-700 and the improved NRR performance of the corresponding HAT-700-A, the chemical structure of the active sites formed during electrochemical etching was investigated. At first, the concentration of nitrogen-containing species in electrolyte increased significantly after the CV etching, which indicates the removal of soluble nitrogen species from HAT-700 during activation. In contrast, the increase for HAT-950 is rather limited as proven by the intensity variation in the UV–Vis spectra of the electrolyte before and after CV etching (Figure S22, Supporting Information). Furthermore, if the HCl electrolyte is replaced with phosphate buffer solution (PBS with pH = 7.2), neither an increase of the response current nor a notable concentration of nitrogen-containing species in the electrolyte can be observed under otherwise similar conditions

(Figure S23, Supporting Information). This confirms that an electrochemical potential and an acidic environment are both necessary to enable the electrochemical etching process. EA analysis of the chemical composition of HAT-700 after CV etching shows that the N-content of is reduced by 5.4 at% (Table S2, Supporting Information). Meanwhile, the C-content decreases by 6.6 at%. Accordingly, XPS results also revealed drops of nitrogen content by 6.6 at%. If the concentration of removed nitrogen species detected in electrolyte is set in relation to the standard curve of ammonium, the calculated etched nitrogen content would correspond to 4.9 at%, which is in good accordance with the EA and XPS results (Table S3, Supporting Information). Because of the etching of nitrile groups, the C/N atomic ratio of HAT-700 increases from 1.94 to 2.24. In contrast, there is no notable decrease of the nitrogen content in HAT-950 after the CV experiment.

We subsequently employed XPS to investigate the change of the chemical environment of HAT-Ts during the electrochemical etching process (survey spectra, **Figure 3**a). In the high-resolution N 1s spectra of HAT-700-A (Figure 3b), the peak corresponding to electron-rich nitrogen has a slight positive shift of 0.8 eV compared to HAT-700, indicating that the remaining nitrogen changes to a higher average formal oxidation state. Furthermore, the content of electron-rich nitrogen at lower binding energies (red line) is slightly decreasing in relation to graphitic-N centered at 401.2 eV (blue line) and oxidized-N centered at 402.7 eV (green line) but still represents the majority of all nitrogen in the material. This observation corroborates our hypothesis that the elevated concentration of nitrogen-containing species in the electrolyte originates from the cleavage of nitrile groups and that the majority of the remaining electron-rich nitrogen atoms are pyrazinic. The electronic state change of HAT-700 also becomes obvious in the C 1s spectra (Figure 3c). Accompanied by the loss of the −CN group, the shape of the C 1s peak undergoes a significant change and

the increasing relative contribution of C=C bonds centered at BE(C 1s) = 284.8 eV (red component) can be observed. Accordingly, the content of electron-rich carbon has an increase to 42.7 at% of all carbon species detected. Notably, the carbon atoms with a binding energy of BE(C 1s) = 292.1 eV can be attributed to −CF$_x$ introduced by the Nafion^{TM} used during the electrode preparation process (Figure S24, Supporting Information).[31] The small doublet located at 440 eV in the survey spectrum of HAT-700-A (Figure 3a) can be attributed to the indium foil applied as sample support during XPS. On the contrary, the C 1s and N 1s spectra of HAT-950 remain the original characteristics after electrochemical etching besides the inevitable −CF$_x$ peak (Figure S25, Supporting Information). In contrast to XPS data, the Raman spectra of HAT-Ts (Figure S26, Supporting Information) do not show significant changes before and after electrochemical activation. This is reasonable, as the loss of nitrile groups would neither affect the D-band nor the G-band which originate from vibrations of the sp^2 carbon six-rings and C=C bonds, respectively. The pore structures of HAT-700 and HAT-700-A before and after electrochemical activation were also evaluated. Their CO$_2$ physisorption behavior is comparable, which indicates that the pore structure of HAT-700 undergoes limited change after electrochemical activation (Figure S27, Supporting Information). According to the analysis given above, it can be concluded that etching under electrochemical potential removes the nitrile groups under acidic environment, while it also endows the material with new edge sites. It is proposed that these sites contain carbon radicals, stabilized by the unique conjugated system of HAT-700 and the remaining heteroatoms. The presence of carbon radicals is proven by electron paramagnetic resonance (EPR) spectra. A comparison between HAT-700 and HAT-700-A shows an obviously enhanced EPR signal at g = 2.027,[32] which can be attributed to unpaired electrons on exposed carbon radicals (Figure S28, Supporting Information). The signal intensity has an apparent decrease after HAT-700-A was left in air for a while due to the annihilations of the formed radical sites. Such carbon radicals are known to be suitable to function as catalytic sites for various reactions, including nitrogen fixation.[23e,33] In addition, another C$_2$N-type material with high pyrazinic nitrogen content but without terminal nitrile groups was also employed for NRR as a reference material (700 °C was chosen as the condensation temperature in analogy to HAT-700).[24b] No similar activation process and nitrogen activation activity were observed (Figure S29, Supporting Information).

In order to illuminate the origin of the remarkable catalytic activity of HAT-A-700, the NRR mechanism on the electrochemically induced catalytically active carbon sites was investigated with theoretical support. Electrochemical detachment of the −CN edge groups from C$_2$N likely forms a carbon radical site stabilized by the large aromatic rings and remaining heteroatoms. Hence, catalytic pathways of NRR promoted by the formed radical (Figure S30, Supporting Information) were investigated using density functional theory (DFT). The distal and alternating pathways via end-on coordination, and the enzymatic pathway by side-on adsorption of N$_2$ on catalytic centers have been calculated in detail. To facilitate the reaction, electron polarization has been proposed to break the N≡N bond via the strong-weak electron polarization on the side-on
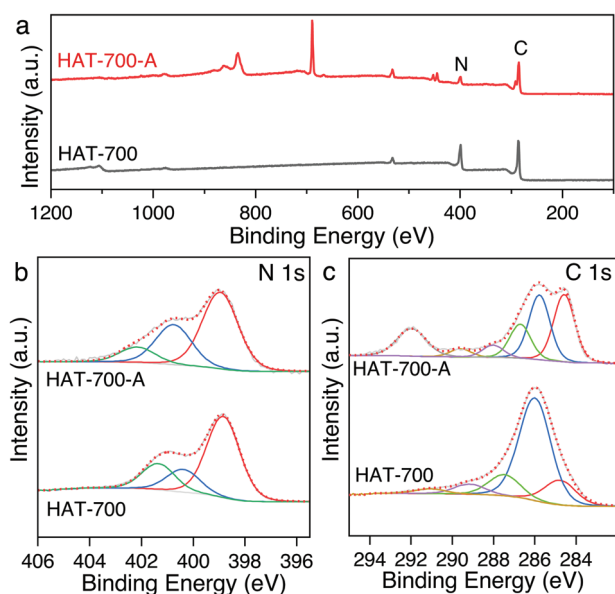
Figure 3. Electronic structure analysis of HAT-700 before and after electrochemical activation a) survey spectra, b) high-resolution deconvoluted N 1s spectrum, and c) C 1s spectrum of HAT-700 and HAT-700-A.
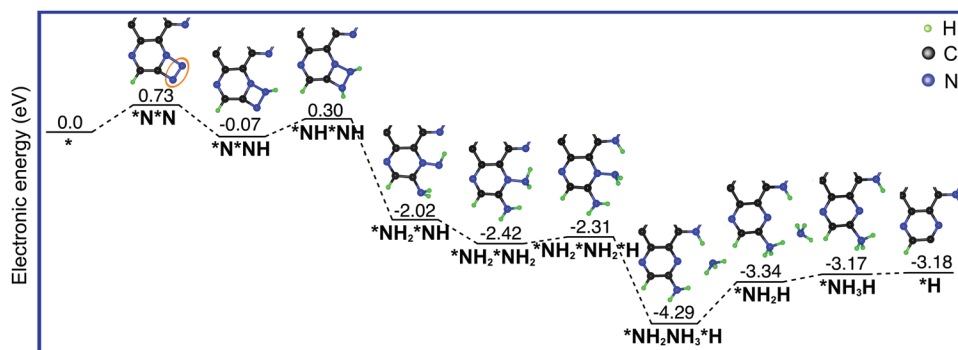
Figure 4. The energy panel of the enzymatic pathway through side-on adsorption of N_2 on the sp^2-carbon and its neighboring nitrogen atom. The adsorbed N_2 has been marked with a brown circle.

adsorbed N_2 molecule.[10b,25] The carbon radical and its adjacent N atom have different electronic structure and could cooperatively activate the N≡N bond. Therefore, the enzymatic pathway was computed through side-on adsorption of N_2 on the sp^2-C and its neighboring N atom (**Figure 4**).[34] The N_2 adsorption on the carbon and nitrogen atoms leads to a square geometry (Figure S30, Supporting Information). This N_2 adsorption is unfavorable with an uphill free energy of 0.73 eV, which could be caused by the electron-rich nitrogen atom in the aromatic rings. However, the different polarization of carbon and nitrogen atoms facilitates the third protonation process, featuring the breaking of the N-N bond and a large decrease in free energy of 2.32 eV. The initial activation barrier of 0.73 eV is in good accordance with the experimentally determined ideal potential in the range of −0.6 to −0.7 V versus RHE. During the fifth protonation the hydrogen atom prefers to adsorb on the nitrogen atom nearby the *NH₂. In the following step, formation of the first ammonia molecule is energetically favorable. The last protonation to form the second ammonia has the highest uphill free energy of 0.95 eV during the entire catalytic processes and is the potential rate-determining step. The successive exothermic reaction steps with low Gibbs energy barrier will account for the excellent catalytic performance for NRR. With the end-on adsorption of the N_2 molecule, the highest uphill free energy (2.04 eV) in the distal pathway is the last protonation. In contrast, it is the fourth protonation (1.78 eV) in alternating pathways (Figure S31, Supporting Information). Moreover, in solution, the neighboring carbon of the sp^2-C could be saturated with −CN, and −OH groups, suggesting multiple possible catalytic pathways (Figures S32 and S33, Supporting Information). However, these pathways lead to relatively high energy barriers. Herein, the adjacent nitrogen of sp^2-C efficiently activates the N-N bond and makes synergy of two neighboring atoms within a suitable distance promotes the catalytic NRR with low energy barrier. In situ technologies to monitor the reactants and intermediates on the materials surfaces is still encouraged in the future to get a more reliable understanding of the mechanism.[35] The pristine HAT-700 without activation was also considered (Figure S34, Supporting Information), but after optimization, the N_2 molecule is desorbed from the −CN group and the pyrazinic N atom of the C_2N. This indicates that the NRR on the inactivated C_2N material is thermodynamically infeasible and that the formation of

carbon radicals after electrochemical activation can be seen as a reasonable origin for the electrocatalytic activity.

3. Conclusion

A series of nitrogen-rich carbon materials was employed for electrochemical nitrogen reduction and the electrochemical activation of HAT-700 was established to introduce catalytically active sites. Such an etching process endowed HAT-700 with improved NRR activity with a maximum Faradaic Efficiency of 11.4% and NH_3 production rate of 5.86 µg mg$^{-1}_{cat}$ h^{-1}. Investigations based on different methods revealed that the electrochemically fragile nitrile groups at the edges of C_2N were removed by electrochemical etching, and then the formed carbon radicals can act as active sites for NRR. A computational model supports the assumption that local carbon radical structure with the adjacent nitrogen can be a cooperatively operating system for nitrogen reduction with low energy barrier. This work provides a new perspective on the origin of catalytically active edge sites in nitrogen-rich carbons generated by an electrochemical activation process. In the future, advanced in situ characterization tools can be applied in order to clarify the mechanisms of nitrogen fixation with the involved elementary steps and to directly confirm the radical structure of active sites under working conditions. A more detailed investigation of the influence of the pore structure on the catalytic properties under working conditions will also be necessary in the future. The work is one of the first attempts to tailor the chemical architecture of carbon-based materials by means of electrochemistry, which may guide the design of metal-free catalysts other than C_2N for potential electrochemical applications even beyond NRR.

Supporting Information

Supporting Information is available from the Wiley Online Library or from the author.

Acknowledgements

ADVANCED
SCIENCE NEWS
www.advancedsciencenews.com

NANO · MICRO
small
www.small-journal.com

Conflict of Interest

The authors declare no conflict of interest.

Data Availability Statement

The data that support the findings of this study are available from the corresponding author upon reasonable request.

Keywords

[1] a) D. R. MacFarlane, P. V. Cherepanov, J. Choi, B. H. R. Suryanto, R. Y. Hodgetts, J. M. Bakker, F. M. F. Vallana, A. N. Simonov, *Joule* **2020**, *4*, 1186; b) A. J. Martín, T. Shinagawa, J. Pérez-Ramírez, *Chem* **2019**, *5*, 263.

[2] a) J. W. Erisman, M. A. Sutton, J. Galloway, Z. Klimont, W. Winiwarter, *Nat. Geosci.* **2008**, *1*, 636; b) B. M. Hoffman, D. Lukoyanov, Z. Y. Yang, D. R. Dean, L. C. Seefeldt, *Chem. Rev.* **2014**, *114*, 4041; c) A. Valera-Medina, H. Xiao, M. Owen-Jones, W. I. F. David, P. J. Bowen, *Prog. Energy Combust. Sci.* **2018**, *69*, 63; d) X. Zhang, B. B. Ward, D. M. Sigman, *Chem. Rev.* **2020**, *120*, 5308.

[3] Y. Wang, T. J. Meyer, *Chem* **2019**, *5*, 496.

[4] a) A. J. Medford, M. C. Hatzell, *ACS Catal.* **2017**, *7*, 2624; b) N. Gilbert, *Nature* **2012**, *483*, 525.

[5] a) R. F. Service, *Science* **2014**, *345*, 610; b) J. G. Chen, R. M. Crooks, L. C. Seefeldt, K. L. Bren, R. M. Bullock, M. Y. Darensbourg, P. L. Holland, B. Hoffman, M. J. Janik, A. K. Jones, M. G. Kanatzidis, P. King, K. M. Lancaster, S. V. Lymar, P. Pfromm, W. F. Schneider, R. R. Schrock, *Science* **2018**, *360*, eaar6611.

[6] a) B. A. Eugene, E. van Tamelen, *J. Am. Chem. Soc.* **1968**, *90*, 4492; b) E. E. Van Tamelen, D. A. Seeley, *J. Am. Chem. Soc.* **1969**, *91*, 5194; c) V. Kyriakou, I. Garagounis, A. Vourros, E. Vasileiou, M. Stoukides, *Joule* **2020**, *4*, 142; d) G. Qing, R. Ghazfar, S. T. Jackowski, F. Habibzadeh, M. M. Ashtiani, C. P. Chen, M. R. Smith 3rd, T. W. Hamann, *Chem. Rev.* **2020**, *120*, 5437; e) J. Deng, J. A. Iniguez, C. Liu, *Joule* **2018**, *2*, 846; f) Q. Qin, M. Oschatz, *ChemElectroChem* **2020**, *7*, 878.

[7] a) C. J. M. van der Ham, M. T. M. Koper, D. G. H. Hetterscheid, *Chem. Soc. Rev.* **2014**, *43*, 5183; b) X. Y. Cui, C. Tang, Q. Zhang, *Adv. Energy Mater.* **2018**, *8*, 1800369; c) B. H. R. Suryanto, H. L. Du, D. B. Wang, J. Chen, A. N. Simonov, D. R. MacFarlane, *Nat. Catal.* **2019**, *2*, 290; d) C. Choi, G. H. Gu, J. Noh, H. S. Park, Y. Jung, *Nat. Commun.* **2021**, *12*, 4353; e) T. Wu, M. M. Melander, K. Honkala, *ACS Catal.* **2022**, *12*, 2505.

[8] a) F. L. Zhou, L. M. Azofra, M. Ali, M. Kar, A. N. Simonov, C. McDonnell-Worth, C. H. Sun, X. Y. Zhang, D. R. MacFarlane,

[9] a) S. Y. Wang, F. Ichihara, H. Pang, H. Chen, J. H. Ye, *Adv. Funct. Mater.* **2018**, *28*, 1803309; b) C. H. Yang, Y. T. Zhu, J. Q. Liu, Y. C. Qin, H. Q. Wang, H. L. Liu, Y. N. Chen, Z. C. Zhang, W. P. Hu, *Nano Energy* **2020**, *77*, 105126; c) N. Lazouski, Z. J. Schiffer, K. Williams, K. Manthiram, *Joule* **2019**, *3*, 1127; d) W. Guo, K. Zhang, Z. Liang, R. Zou, Q. Xu, *Chem. Soc. Rev.* **2019**, *48*, 5658.

[10] a) C. Lv, Y. Qian, C. Yan, Y. Ding, Y. Liu, G. Chen, G. Yu, *Angew. Chem., Int. Ed.* **2018**, *57*, 10246; b) J. Li, S. Chen, F. J. Quan, G. M. Zhan, F. L. Jia, Z. H. Ai, L. Z. Zhang, *Chem* **2020**, *6*, 885; c) J. Liu, X. Kong, L. Zheng, X. Guo, X. Liu, J. Shui, *ACS Nano* **2020**, *14*, 1093; d) S. J. Li, D. Bao, M. M. Shi, B. R. Wulan, J. M. Yan, Q. Jiang, *Adv. Mater.* **2017**, *29*, 1700001; e) Y. X. Guo, Z. Y. Yao, S. Q. Zhan, B. J. J. Timmer, C. W. Tai, X. Y. Li, Z. Xie, Q. J. Meng, L. Z. Fan, F. G. Zhang, M. S. G. Ahlquist, M. Cuartero, G. A. Crespo, L. C. Sun, *Nano Energy* **2020**, *78*, 105391; f) Y. T. Liu, L. Tang, J. Dai, J. Yu, B. Ding, *Angew. Chem., Int. Ed.* **2020**, *59*, 13623; g) D. Z. Yao, C. Tang, L. Q. Li, B. Q. Xia, A. Vasileff, H. Y. Jin, Y. Z. Zhang, S. Z. Qiao, *Adv. Energy Mater.* **2020**, *10*, 2001289; h) Y.-C. Hao, Y. Guo, L.-W. Chen, M. Shu, X.-Y. Wang, T.-A. Bu, W.-Y. Gao, N. Zhang, X. Su, X. Feng, J.-W. Zhou, B. Wang, C.-W. Hu, A.-X. Yin, R. Si, Y.-W. Zhang, C.-H. Yan, *Nat. Catal.* **2019**, *2*, 448; i) Q. Qin, Y. Zhao, M. Schmallegger, T. Heil, J. Schmidt, R. Walczak, G. Gescheidt-Demner, H. Jiao, M. Oschatz, *Angew. Chem., Int. Ed.* **2019**, *58*, 13101; j) W. Y. Zhang, W. J. Lin, J. Ren, N. F. Zheng, B. H. Wu, *ChemElectroChem* **2022**, *9*, 202100052.

[11] a) H. Liu, N. Guijarro, J. Luo, *J Energy Chem* **2021**, *61*, 149; b) H. D. Shen, C. Choi, J. Masa, X. Li, J. S. Qiu, Y. Jung, Z. Y. Sun, *Chem* **2021**, *7*, 1708.

[12] W. Bi, N. Shaigan, A. Malek, K. Fatih, E. Gyenge, D. P. Wilkinson, *Energy Environ. Sci.* **2022**, *15*, 2259.

[13] a) J. Choi, H.-L. Du, M. Chatti, B. H. R. Suryanto, A. N. Simonov, D. R. MacFarlane, *Nat. Catal.* **2022**, *5*, 382; b) Y.-C. Hao, L.-W. Chen, A.-X. Yin, *Nat. Catal.* **2022**, *5*, 385.

[14] M. Kolen, D. Ripepi, W. A. Smith, T. Burdyny, F. M. Mulder, *ACS Catal.* **2022**, *12*, 5726.

[15] a) X. Liu, L. M. Dai, *Nat. Rev. Mater.* **2016**, *1*, 16064; b) L. Dai, D. W. Chang, J. B. Baek, W. Lu, *Small* **2012**, *8*, 1130; c) Q. Qin, T. Heil, J. Schmidt, M. Schmallegger, G. Gescheidt, M. Antonietti, M. Oschatz, *ACS Appl. Energy Mater.* **2019**, *2*, 8359; d) Y. Zhao, L. Yan, X. Zhao, *ChemElectroChem* **2022**, *9*, 202101126.

[16] a) Y. Liu, Q. Li, X. Guo, X. Kong, J. Ke, M. Chi, Q. Li, Z. Geng, J. Zeng, *Adv. Mater.* **2020**, *32*, 1907690; b) X. Yu, P. Han, Z. Wei, L. Huang, Z. Gu, S. Peng, J. Ma, G. Zheng, *Joule* **2018**, *2*, 1610.

[17] M. Antonietti, M. Oschatz, *Adv. Mater.* **2018**, *30*, 1706836.

[18] a) G. Peng, J. Wu, M. Wang, J. Niklas, H. Zhou, C. Liu, *Nano Lett.* **2020**, *20*, 2879; b) H. Wang, Y. Shao, S. Mei, Y. Lu, M. Zhang, J. K. Sun, K. Matyjaszewski, M. Antonietti, J. Yuan, *Chem. Rev.* **2020**, *120*, 9363.

[19] a) S. Z. Andersen, V. Colic, S. Yang, J. A. Schwalbe, A. C. Nielander, J. M. McEnaney, K. Enemark-Rasmussen, J. G. Baker, A. R. Singh, B. A. Rohr, M. J. Statt, S. J. Blair, S. Mezzavilla, J. Kibsgaard, P. C. K. Vesborg, M. Cargnello, S. F. Bent, T. F. Jaramillo, I. E. L. Stephens, J. K. Norskov, I. Chorkendorff, *Nature* **2019**, *570*, 504; b) Y. Zhao, R. Shi, X. Bian, C. Zhou, Y. Zhao, S. Zhang, F. Wu, G. I. N. Waterhouse, L. Z. Wu, C. H. Tung, T. Zhang, *Adv. Sci.* **2019**, *6*, 1802109; c) H. Iriawan, S. Z. Andersen, X. Zhang, B. M. Comer, J. Barrio, P. Chen, A. J. Medford, I. E. L. Stephens, I. Chorkendorff, Y. Shao-Horn, *Nat. Rev. Methods Primers* **2021**, *1*, 56; d) J. Choi, B. H. R. Suryanto, D. Wang, H. L. Du, R. Y. Hodgetts, F. M. Ferrero Vallana, D. R. MacFarlane, A. N. Simonov, *Nat. Commun.* **2020**, *11*, 5546.

[20] Y. Fang, Z. Liu, J. Han, Z. Jin, Y. Han, F. Wang, Y. Niu, Y. Wu, Y. Xu, *Adv. Energy Mater.* **2019**, *9*, 1803406.

[21] C. Lv, C. Yan, G. Chen, Y. Din g, J. Sun, Y. Zhou, G. Yu, *Angew. Chem., Int. Ed.* **2018**, *57*, 6073.

[22] a) K. Kishida, M. Kitano, M. Sasase, P. V. Sushko, H. Abe, Y. Niwa, K. Ogasawara, T. Yokoyama, H. Hosono, *ACS Appl. Energy Mater.* **2020**, *3*, 6573; b) M. Oschatz, T. W. van Deelen, J. L. Weber, W. S. Lamme, G. Wang, B. Goderis, O. Verkinderen, A. I. Dugulan, K. P. de Jong, *Catal. Sci. Technol.* **2016**, *6*, 8464.

[23] a) N. Han, Y. Wang, H. Yang, J. Deng, J. Wu, Y. Li, Y. Li, *Nat. Commun.* **2018**, *9*, 1320; b) C. Y. Hu, Q. Y. Ma, S. F. Hung, Z. N. Chen, D. H. Ou, B. Ren, H. M. Chen, G. Fu, N. F. Zheng, *Chem* **2017**, *3*, 122; c) Z. Zou, T. Wang, X. Zhao, W.-J. Jiang, H. Pan, D. Gao, C. Xu, *ACS Catal.* **2019**, *9*, 7356; d) X. Shang, B. Dong, Y.-M. Chai, C.-G. Liu, *Sci. Bull.* **2018**, *63*, 853; e) R. K. Das, Y. Wang, S. V. Vasilyeva, E. Donoghue, I. Pucher, G. Kamenov, H. P. Cheng, A. G. Rinzler, *ACS Nano* **2014**, *8*, 8447.

[24] a) J. Mahmood, E. K. Lee, M. Jung, D. Shin, I. Y. Jeon, S. M. Jung, H. J. Choi, J. M. Seo, S. Y. Bae, S. D. Sohn, N. Park, J. H. Oh, H. J. Shin, J. B. Baek, *Nat. Commun.* **2015**, *6*, 6486; b) N. Fechler, N. P. Zussblatt, R. Rothe, R. Schlögl, M.-G. Willinger, B. F. Chmelka, M. Antonietti, *Adv. Mater.* **2016**, *28*, 1287; c) R. Walczak, A. Savateev, J. Heske, N. V. Tarakina, S. Sahoo, J. D. Epping, T. D. Kühne, B. Kurpil, M. Antonietti, M. Oschatz, *Sustainable Energy Fuels* **2019**, *3*, 2819.

[25] R. Walczak, B. Kurpil, A. Savateev, T. Heil, J. Schmidt, Q. Qin, M. Antonietti, M. Oschatz, *Angew. Chem., Int. Ed.* **2018**, *57*, 10765.

[26] a) L. Q. Li, C. Tang, Y. Zheng, B. Q. Xia, X. L. Zhou, H. L. Xu, S. Z. Qiao, *Adv. Energy Mater.* **2020**, *10*, 2000789; b) C. Tang, H.-F. Wang, X. Chen, B.-Q. Li, T.-Z. Hou, B. Zhang, Q. Zhang, M.-M. Titirici, F. Wei, *Adv. Mater.* **2016**, *28*, 6845.

[27] M. Thommes, K. Kaneko, A. V. Neimark, J. P. Olivier, F. Rodriguez-Reinoso, J. Rouquerol, K. S. W. Sing, *Pure Appl. Chem.* **2015**, *87*, 1051.

[28] T. Xing, Y. Zheng, L. H. Li, B. C. Cowie, D. Gunzelmann, S. Z. Qiao, S. Huang, Y. Chen, *ACS Nano* **2014**, *8*, 6856.

[29] a) Q. Yang, Y. Guo, J. Gu, N. Li, C. Wang, Z. Liu, X. Li, Z. Huang, S. Wei, S. Xu, L. Song, J. Fan, Z. Chen, J. Qiu, C. Zhi, *Nano Energy* **2020**, *78*, 105283; b) C. Hu, L. Dai, *Adv. Mater.* **2019**, *31*, 1804672.

[30] L. Zhou, C. E. Boyd, *Aquaculture* **2016**, *450*, 187.

[31] C. Chen, G. Levitin, D. W. Hess, T. F. Fuller, *J. Power Sources* **2007**, *169*, 288.

[32] C. P. L. Prasuna, R. P. S. Chakradhar, J. L. Rao, N. O. Gopal, *Spectrochim. Acta, Part A* **2008**, *71*, 809.

[33] a) A. Gennaro, A. A. Isse, J.-M. Savéant, M.-G. Severin, E. Vianello, *J. Am. Chem. Soc.* **1996**, *118*, 7190; b) B. M. Comer, Y.-H. Liu, M. B. Dixit, K. B. Hatzell, Y. Ye, E. J. Crumlin, M. C. Hatzell, A. J. Medford, *J. Am. Chem. Soc.* **2018**, *140*, 15157.

[34] W. Wang, H. Zhang, S. Zhang, Y. Liu, G. Wang, C. Sun, H. Zhao, *Angew. Chem., Int. Ed.* **2019**, *58*, 16644.

[35] a) Y. Tang, Y. Zhang, O. I. Malyi, N. Bucher, H. Xia, S. Xi, Z. Zhu, Z. Lv, W. Li, J. Wei, M. Srinivasan, A. Borgna, M. Antonietti, Y. Du, X. Chen, *Adv. Mater.* **2018**, *30*, 1802200; b) Y. Zhao, F. Li, W. Li, Y. Li, C. Liu, Z. Zhao, Y. Shan, Y. Ji, L. Sun, *Angew. Chem., Int. Ed.* **2021**, *60*, 20331.